Journal of MATERIALS RESEARCH

Invited Paper
DOI:10.1557/s43578-022-00530-4

Density functional study of Ga intercalation at graphene/SiC heterointerface

Nadire Nayir[1,2,a)]

[1] Department of Physics, Karamanoglu Mehmetbey University, Karaman 70000, Turkey
[2] Department of Mechanical Engineering and 2-Dimensional Crystal Consortium (2DCC) Materials Research Institute, The Pennsylvania State University, University Park, PA 16802, USA
[a)] Address all correspondence to this author. e-mail: nnayir@kmu.edu.tr; nzn36@psu.edu

Received: 9 December 2021; accepted: 28 February 2022; published online: 15 March 2022

The intercalation technique has harnessed tremendous attention in the 2D materials' community, enabling to fabricate atomically thin and stable non-layered materials such as Ga at the heterointerface of graphene/SiC. However, the atomistic mechanism of the metal intercalation at such interface has still yet to been understood. In this study, first-principles calculations provide a thermodynamic and kinetic level understanding of the Ga penetration into and nucleation at the SiC/graphene interface. A Ga atom encapsulated at the graphene/SiC interface is thermodynamically more stable than adsorbed on the top of the graphene layer, signifying the necessity of exploiting the SiC substrate during the 2D Ga growth to facilitate the Ga migration into the SiC/graphene interface. Additionally, the sizes of a Ga atom and vacancy defect are critical to the Ga penetration through graphene, affecting the thermodynamic and kinetic preference of a Ga atom between the adsorption on graphene or the intercalation in to the SiC/graphene gallery.

Introduction

Fabrication of atomically thin non-layered materials is quite challenging compared to van der Waals structures because in-plane interactions within a non-layered material are dominantly governed by chemical bonds which are difficult to break without sacrificing the crystal quality [1, 2]. Direct epitaxy of non-layered materials (e.g., GaN, InN, Pb) on lattice-mismatched substrates are strain-driven and results in 3D islands as a consequence of the combined effect of the Volmer-Weber and Stranski–Krastanov growth modes [3–8]. Alternatively, taking advantage of the Frank-van der Merwe growth mode [9, 10], recent experimental studies offer an intercalation technique that enables to grow 2D-nonlayered materials atom by atom by encapsulating them at the half van der Waals interface of epitaxial graphene (EG) and substrate (e.g., silicon carbide (SiC)) where EG is used as a cap layer to stabilize intercalants at the interface [3–17]. The synthesis of large area and high-quality EG on SiC substrates by the depletion of Si atoms is one of the most-used applications [3, 4]—the thermal treatment of Si-terminated SiC (0001) leads to the sublimation of the silicon surface atoms that leave behind a C-rich surface. The rearrangement of the remaining C atoms leads to the $(6\sqrt{3}\times 6\sqrt{3})R30^{\circ}$ surface reconstruction, called a buffer or zero layer. Upon the hydrogenation, the buffer layer transforms into an sp^2 hybridized quasi-free-standing EG layer [3, 11, 18, 19] which is still partially bound to the SiC surface. During the fabrication of EG, the formation of lattice defects is inevitable. The common intrinsic defects imaged in graphene sheets can be categorized into Stone–Wales defects, single vacancy defects, multivacancy defects [11, 20–25]. Because of the dangling bonds (e.g., vacancy defects) present on the EG layer, EG still chemically interacts with the SiC substrate. Ga atoms diffusing through EG accumulate at the interface to form a 2D Ga film. Several studies show that graphene impurities such as defects, wrinkles, step edges are expected to play a crucial role during the Ga intercalation, acting as a local gate for Ga penetration through graphene, similar to the cases for lithium, copper, cesium, hydrogen, and indium [11, 17, 24, 26–32]. Then, Ga metals diffusing through "gates" nucleate and coalesce to form a continuous thin-film. Al Balushi et al. [3] hypothesize that, at the early stages of the nucleation and growth, intercalated metals are mainly localized around graphene impurities such as defects and wrinkles at the interface.

As fabricating a large area and environmentally stable single-crystalline 2D Ga becomes possible, it is more critical to understand the underlying thermodynamic and kinetic mechanism behind (i) the Ga penetration through defects, (ii) nucleation, and (iii) growth at the interface. This has prompted the need for atomic-scale simulations that can help guide the synthesis of 2D Ga with a controllable thickness. Several theoretical studies have been devoted to investigating the molecular-level mechanism of the EG fabrication on SiC and the metal penetration through graphene with/without a SiC substrate underneath. Zhang et al. [33] provide a detailed atomistic mechanism on the growth of an sp^2 structured EG on the SiC substrate by the sublimation of Si surface atoms at the ReaxFF level. A recent study at the ReaxFF level also shows that multivacancy defects catalyze the Ga intercalation through a free-standing graphene layer by lowering the kinetic barrier encountered during the Ga penetration, thereby lowering the growth temperature required for the 2D Ga fabrication [24]. This phenomenon is also reported for a Cu and Dy atom and it is demonstrated that the geometry of the entry portal which can be either step edges with high adsorption sites or multivacancies plays a critical role in lowering the energy barrier of the atom intercalation through graphene [25, 28]. As a relevant study, Briggs et al. [11] show that plasma-induced larger vacancy defects in a free-standing graphene layer are effective players during the adsorption and desorption of Ga on graphene, suggesting the routes toward using atomic-scale defect engineering to control the Ga intercalation. The same work also explored the calculated crystal phase of a continuous trilayer Ga film at the interface where the first, second, and third layers of the Ga film are found thermodynamically stable on the top of Si, carbon (Ga_C), and hollow (Ga_{hollow}) sites of the SiC surface, and the crystal phase of the Ga film shows the resemblance to the metastable distorted fcc phase of Ga(III) [34]. Several works also focused on the Li penetration through a free-standing graphene layer, suggesting that a relatively light Li atom compared to Ga can pass through the defects larger than a single vacancy [17, 27]. Another Cu-based study shows that the topological evolution of 5–8–5 to divacancy reduces the potential barrier for the Cu penetration through graphene and the existence of SiC substrate underneath graphene stabilizes the intercalated Cu atom at the interface [26]. However, to the author's best knowledge, there is no report yet on the atomic-level investigation of the combined effect of graphene defects and the SiC substrate on the 2D Ga growth even though the SiC substrate is a significant component of the intercalation mechanism. Additionally, despite the significant progress on 2D Ga growth at the SiC/graphene heterointerface, a clear atomic-level understanding of the penetration and nucleation mechanism is still lacking.

In this study, the density functional calculations were conducted to uncover the complex interplay between vacancy defects of graphene and the SiC substrate during the Ga penetration, and to shed light into the Ga nucleation mechanism at the interface. Four representative graphene models, single vacancy (SV), divacancy (DV), and reconstructed divacancies (5–8–5 and 555–777) were adopted in the calculations. Then, the Ga adsorption/penetration on/through defect was investigated in the absence of the SiC substrate to determine the thermodynamically and kinetically allowable defect models for the Ga diffusion through a free-standing graphene model. Subsequently, to identify the thermodynamically stable nucleation site for Ga on the SiC substrate, the single-atom model was adopted where an isolated Ga atom was introduced on the different symmetry-allowed sites (T1, T4, H3, and BC) of a Si-terminated SiC surface in the absence/presence of a cap layer of graphene. Then, the migration pathway of Ga into the SiC/graphene gallery was explored from thermodynamic and kinetic aspects.

Results and discussion

Ga on a free-standing graphene

First-principles calculations were conducted to investigate first the atomistic mechanism of Ga intercalation through a free-standing graphene layer. To this end, four representative topological defect models, single vacancy (SV), divacancy (DV), and reconstructed divacancies (5–8–5 and 555–777) were built by the removal of carbon atoms from the center of a 6×6 hexagonal pristine graphene sheet with the dimensions of $14.76\times14.76\times20$ A^3 [Fig. 1(a)]. Note that the 5–8–5 defect is composed of two pentagonal and one octagonal rings while the 555–777 defect contains three pentagonal and three heptagonal rings. Subsequently, a Ga atom was deposited on optimized pristine and defective models, then the models were allowed to relax into their ground states [Fig. 1(b)]. The adsorption energy, E_{ads}, of a Ga atom on graphene was computed based on the equation of $E_{ads} = (E_{Ga+graphene} + (E_{graphene} + E_{Ga})$ where $E_{graphene+Ga}$ is the total energy of graphene with a Ga atom adsorbed. $E_{graphene}$ and E_{Ga} are the energies of a graphene sheet and an isolated Ga atom in a vacuum, respectively.

As depicted in Fig. 1(c), the adsorption of a Ga atom on the graphene sheet is an exothermic process and the existence of defect enhances substantially the binding strength of the Ga atom to the surface. Unreconstructed divacancy, DV interacts strongly with the Ga atom, as well, compared to the reconstructed divacancies (5–8–5 and 555–777). Note that the Jahn Teller distortion is observed in the 5–8–5 and 555–777 membered rings where the bond reconstruction between two C-dangling atoms stabilize the sheet by lowering energy. SV also results in a strong binding strength owing to the presence of C-dangling bonds around the defect, but still slightly lower than DV, signifying the impact of the number of C-dangling bonds on the Ga binding strength.

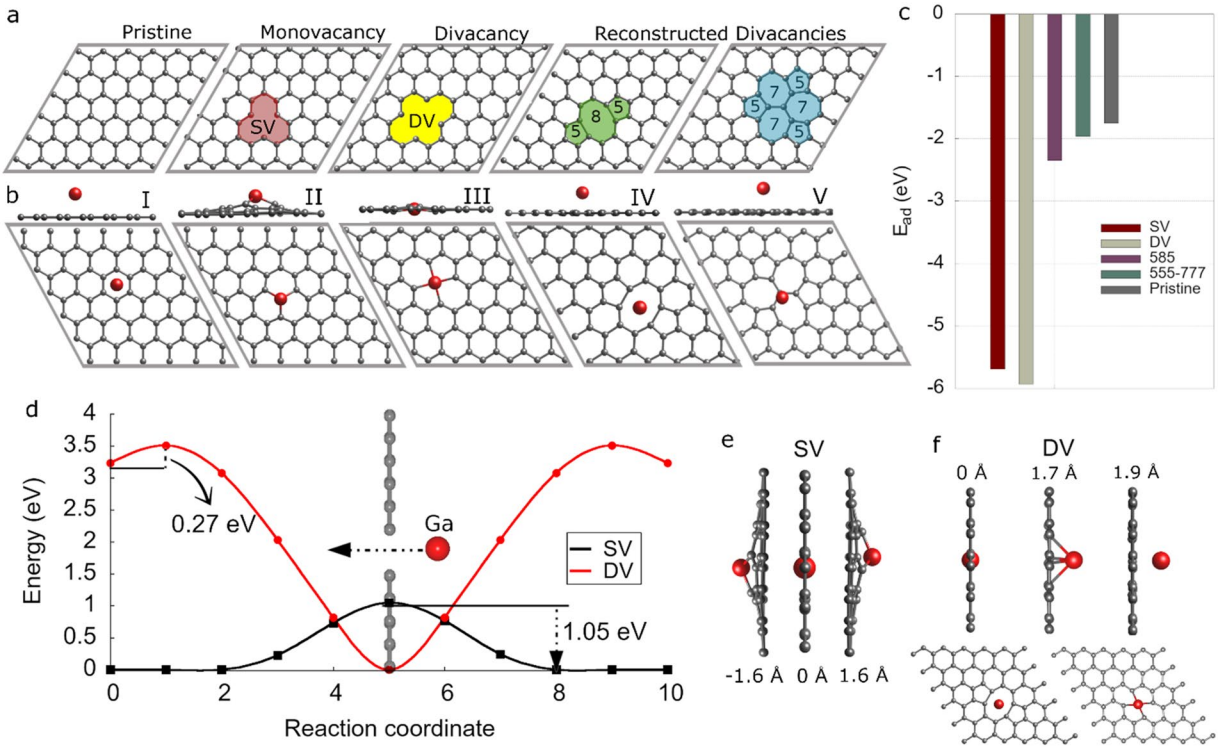

Figure 1: Ball-stick representation of pristine (I), monovacancy (SV) (II), divacancy (DV) (III), 5–8–5 (IV) and 555–777 (V) graphene models (a) without and (b) with an adsorbed Ga atom. (c) The adsorption energies of a Ga atom depending on defect type where a more negative energy value signifies stronger binding of Ga to the surface. (d) The energy barrier for Ga penetration through SV and DV in a free-standing graphene layer. (e), (f) Ball-stick illustration of the Ga migration through SV and DV defects. Ga diffusion realizes from right to left in the graph. During the diffusion, Ga encounters the energy barriers of 1.05 and 0.27 eV at (e) 0 Å and (f) 1.7 Å on the SV and DV models, respectively.

Additionally, the Ga atom chemically binds to SV and DV while interacting weakly with the reconstructed 5–8–5 and 555–777 defects which results in the physisorption of Ga on graphene through van der Waals forces [Fig. 1(b)–(IV)], similar to the pristine case [Fig. 1(b)–(I)]. Akin to the Al and Si-based works [35], the SV model leads to the out-of-plane bonding of a Ga atom on graphene [Fig. 1(b)–(II)]—one can be attributed to the smaller size of the defect than that of a Ga atom whose atomic radius (122 pm [36]) is larger than the atomic radius of C (70 pm [36]), effecting the thermodynamic and kinetic preference of a Ga atom between the adsorption on graphene or the intercalation into the SiC/graphene gallery [37]. Figure 1(d) shows the diffusion dynamics of a Ga atom through a free-standing graphene sheet with an SV and DV defect, which has mirror symmetry with respect to the graphene sheet in the absence of the SiC substrate [26, 27, 38]. The Ga atom encounters a kinetic barrier of 1.05 eV (compared with the barriers of 1.07 and 0.74 eV for Al and Si, respectively [35]) during the penetration through the SV defect [Fig. 1(e)], indicating that the Ga adsorption on top of the SV model is kinetically much more favorable than the intercalation. On the other hand, Ga favors intercalating through the DV defect over to adsorb on top of graphene, exhibiting a nearly barrierless (~ 0.27 eV at 1.7 Å away from graphene) intercalation [Fig. 1(f)]. This indicates that the Ga intercalation through SV is thermodynamically less favorable than the DV model, further kinetically hindered as also reported for Si, Al, and Li [27, 35]. It is noteworthy that, in the proximity of a Ga atom, the 5–8–5 defect transforms to DV by breaking the reconstructed bonds between C-pairs around the defect, called a transition state. During the bond cleavage, an energetic local maximum is observed at around 1.7 Å away from graphene (also around – 1.7 Å). Then, the energy monotonically decreases as Ga approaches the graphene layer and the Ga atom reaches its local minimum conformation when it resides in the defect at 0 Å [Fig. 1(f)].

Deposition of isolated Ga atom on SiC substrate

Surface hydrogenation is a well-established technique that enables the achievement of an unreconstructed SiC surface that stays stable against oxidation [3, 4]. Following the earlier works [39–47], three hexagonal representative models of the bilayer SiC (0001) substrate—non-passivated [*no–H*, Fig. 2(a)-top], H-passivated only bottom [*bottom-H*, Fig. 2(b)-top] and both top and bottom sides (*both-H*, Fig. 2(c)-top) of the substrate—were examined to uncover the impact of the surface

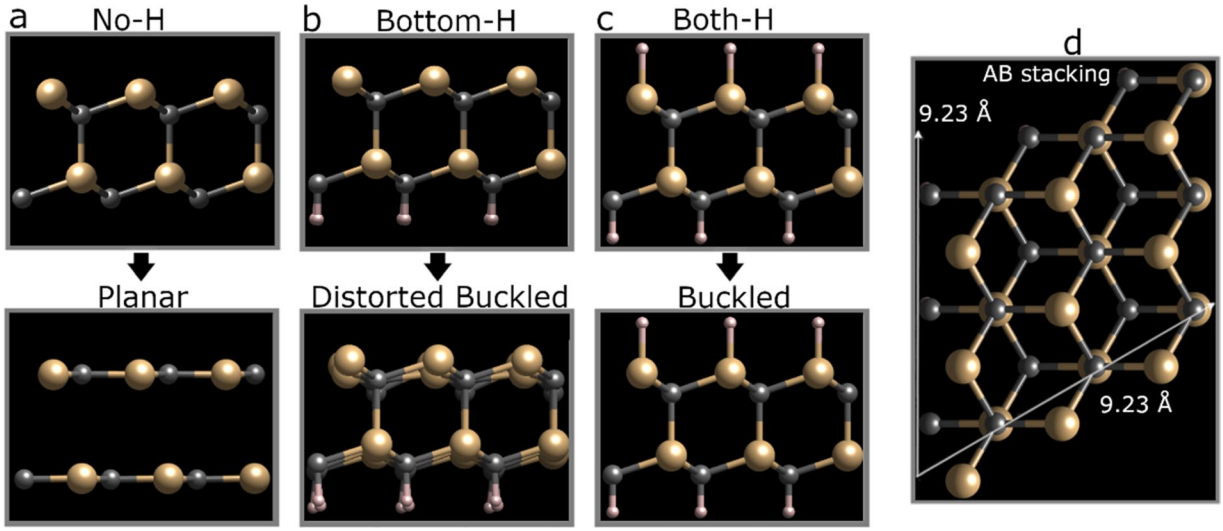

Figure 2: Optimized configurations of (a) non-passivated, (b) only bottom passivated and (c) both sides passivated SiC with hydrogen. Top and bottom images in (a) are before and after the relaxation, respectively. (d) Stacking sequence of SiC with the lateral dimensions of 9.23 × 9.23 Å^2.

termination on the atomic structure of SiC. A vacuum layer of 15 Å was inserted in the direction of normal to the SiC surface. After the structural relaxation, although a bulk SiC exhibits a natural sp^3 bonding [15–18], a non-passivated SiC adopts an sp^2 planar geometry as seen from Fig. 2(a)-bottom and also confirmed by previous studies [19–22]. In the second configuration [Fig. 2(b)-bottom], the SiC substrate partially preserves its symmetry but is still distorted [23]. The fully passivated SiC substrate maintains its buckled sp^3 geometry [Fig. 2(c)-bottom].

Subsequent to the structural relaxation, the metastable site for a single-atom Ga metal deposition on a SiC surface with/without H-passivation was investigated in the absence of a defective graphene layer. For which, a Ga atom was introduced on different symmetry-allowed sites of each SiC substrate (*no–H, bottom-H, and both-H*) as illustrated in Fig. 3(a) where T1, T4, H3, and BC are the intercalation sites for a Ga atom. T1 is a one-fold coordinated site on the topmost Si atom. T4 is a four-fold coordinated hcp site above a carbon atom of the first layer of the SiC substrate. H3 is a three-fold coordinated fcc site above a carbon atom of the second layer. The BC site is a bond-centered site and located between two adjacent silicon atoms. Then, the structures were allowed to structurally relax. As presented in Figs. 3(b–d) and 4, BC, T4, and H3 were found as the most stable site for a Ga atom adsorbed on the *no–H*, *bottom-H*, and *both-H* SiC models, respectively, indicating that Ga atoms are prone to form three-fold sp^2 bonding with surface Si atoms of SiC. Additionally, a Ga atom initially located on BC and T1 on the planar SiC maintains its location while one on T4 and H3 migrates to the most stable BC site [Figs. 3(b), 4(b)]. For the *bottom-H* model, the T1 and BC configurations are converted to T4 and T4-distorted (T4') during the relaxation [Figs. 3(c), 4(c)]. This shows that a Ga atom favorably occupies the T4 site rather than T1 or BC as also reported by earlier DFT studies for Cu and Li atoms [10–12], reasoning also that the T1, BC, and T4 configurations result in the same binding energies in Fig. 4(a). Additionally, in both the T4 and H3 cases, the Ga adatom saturates the three Si-dangling bonds on the surface. In the *both-H* model, the structural relaxation leads to the Ga migration from BC to the most stable H3 site while the rest stabilize themselves at their initial positions [Figs. 3(d), 4(d)]. The Ga-H bond strength in the *both-H* model was also found significantly weaker than that of Ga-Si in the *bottom-H* model [Fig. 4(a)].

Ga intercalation at the graphene/SiC interface

In experiments, a cap layer of graphene stabilizes Ga atoms at the SiC/graphene interface, leading to the thin-film 2D Ga growth [3, 4, 10]. Graphene impurities (e.g., defects, wrinkles) play a crucial role at the early stages of the Ga nucleation and growth, serving as a local gate for Ga to pass into the interface [3, 11, 48]. Additionally, the intercalated Ga atoms mainly nucleate nearby defects, edges, wrinkles as reported by Al Balushi et al. [3]. From this point forward, to uncover the combined impact of SiC substrate and graphene layer on the Ga penetration and nucleation, an optimized graphene with a DV defect was placed onto the optimized SiC model, resulting in a SiC/graphene gallery with an interlayer spacing of 4 Å as depicted in Fig. 3(a), (b).

In this model, the carbon atoms on the bottom layer of the SiC substrate were capped with hydrogen (*bottom-H*) and

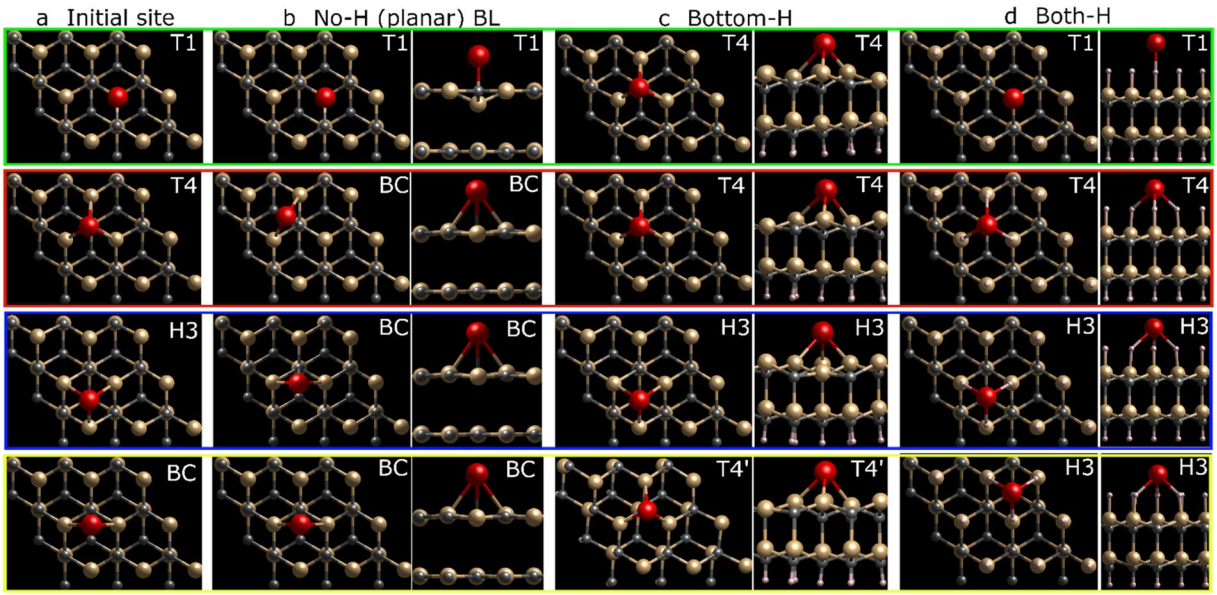

Figure 3: The Ga adsorption on the SiC substrate in the absence of graphene. (a) Initial and (b–d) relaxed configurations of the T1, T4, H3, and BC models. Top (left) and side (right) views of the models in (b) the non-passivated planar (*No–H*), (c) only the bottom passivated buckled (*bottom-H*) and (d) both sides passivated (*both-H*) SiC cases. (b) On the planar sheet, Ga atoms deposited on T4, H3, and BC are relaxed to the BC site while a Ga atom located on T1 stays at the same position. (c) In the *bottom-H* model, Ga on T1 and T4 moves to the T4 site while the H3 model maintains its structure. The BC model results in a distorted T4 model after the structural relaxation. (d) The *both-H* model results in H3 as the most stable intercalation site for Ga. The BC configuration is relaxed to the H3 configuration while T1 and T4 maintain their configurations.

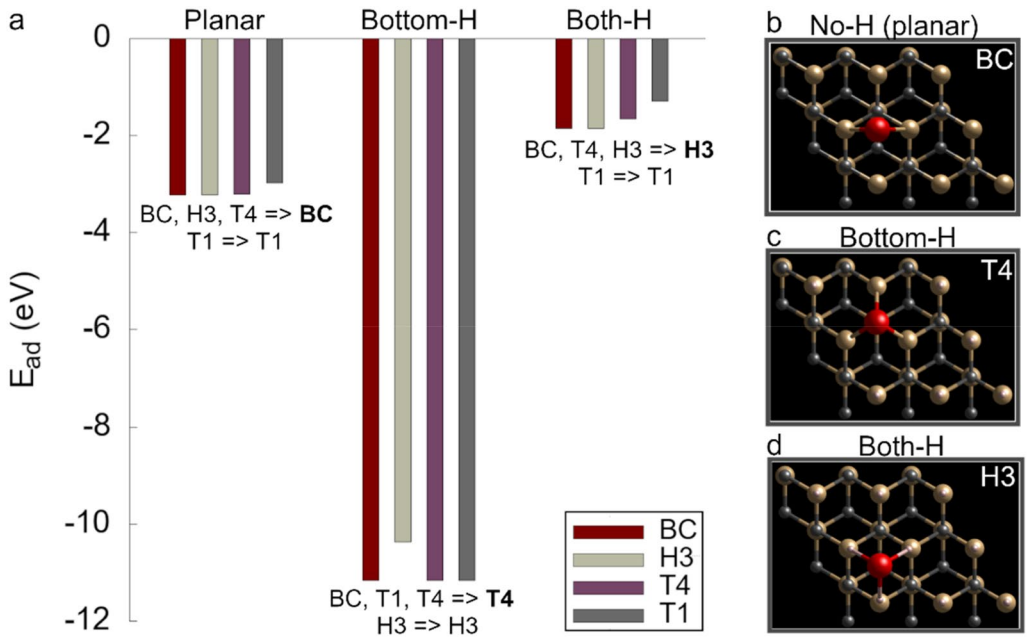

Figure 4: (a) Binding energies of a Ga atom on various (T4, T1, H3, and BC) intercalation sites on the *planar*, the *bottom-H* and *both-H* SiC models and (b)–(d) the corresponding most stable configurations. The energies in (a) are associated with the system including only a single Ga atom and a SiC substrate represented in Fig. 3 where a Ga atom is initially located at T1, T4, H3, and BC intercalation sites of each SiC model. BC, T4, and H3 are determined as the most stable site for (b) *planar*, (c) *bottom-H* and (d) *both-H* SiC models, respectively. Note that, BC and T1 on *planar*, H3 and T4 on *bottom-H* and H3 and T1 on *both-H* SiC models maintain their initial form while a Ga atom initially placed on H3 and T4 sites on *planar*, T1 and BC on the *bottom-H* and BC and T4 on the *both-H* models migrates to the BC (b), T4 (c) and H3 (d) sites, respectively, during energy minimization.

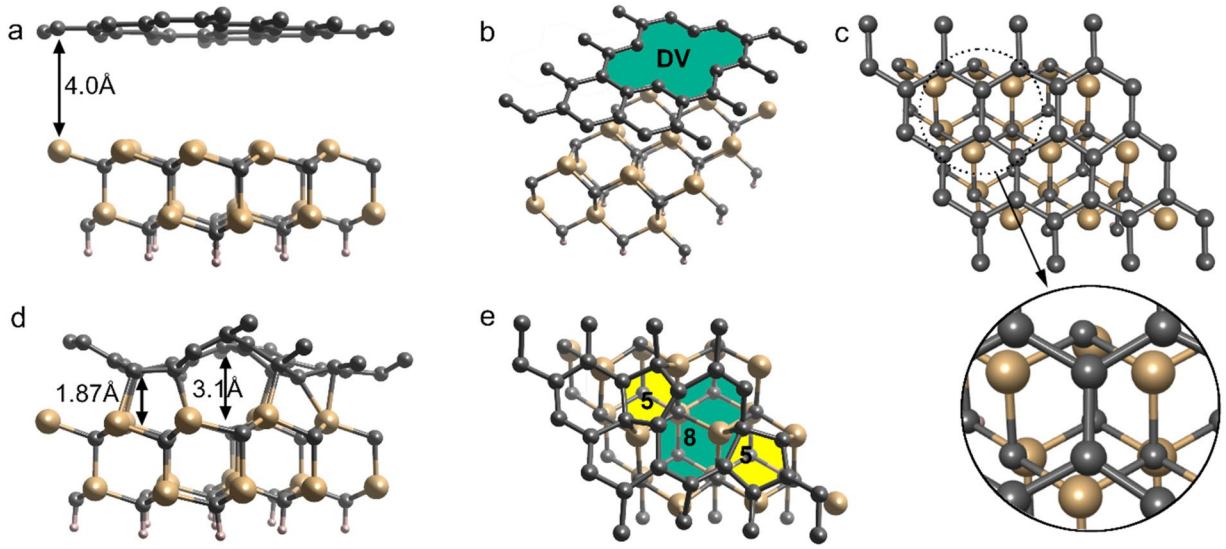

Figure 5: (a) Side and (b) top views of the initial configuration of the model containing the defective graphene with DV and the SiC substrate with an interlayer distance of 4 Å. (c) Top view of the model without defect, where the region circled by a dashed black line is magnified further to depict the non-rotated graphene lattice relative the SiC substrate. (d) Side and (e) top views of the optimized model where the closest and farest distances between graphene and SiC are 1.87 and 3.10 Å, respectively, and the graphene layer is partially bound to the SiC substrate. During the relaxation, DV transformed to a 5–8–5 defect type.

the dangling bonds on the top layer of the substrate were left unsaturated [Fig. 5(a),(b)], thus allowing the graphene sheet to bind to the substrate during the relaxation. Additionally, earlier works [3, 25, 49, 50] report the residual compressive strain in an EG layer grown on SiC because of the thermal lattice mismatch and the $6\sqrt{3}\times6\sqrt{3}R30^{\circ}$ surface reconstruction of SiC during the Si sublimation. However, several theoretical attempts [51, 52] showed that the realistic modeling of the compressive strain in epitaxial graphene requires a commensurate SiC/graphene supercell that should contain more than 1000 atoms (the $6\sqrt{3}\times6\sqrt{3}$ R30 of SiC is exactly commensurate with the 13×13 supercell of graphene) which makes the DFT calculation time-consuming. For the sake of saving the computational cost and mimicking the experimental conditions, the lattice constant of the nonrotated graphene relative to SiC [Fig. 5(c)] was isotropically compressed by 6% to meet the lateral dimensions of the SiC substrate. After the structural relaxation, several carbon atoms in the graphene layer were partially bound to the SiC substrate and the DV defect evolved into a 5–8–5 configuration as seen from Fig. 5(d), (e). Subsequently, three different systems were modeled by trapping a Ga atom at the interface on the T1, T4, and H3 sites of the SiC substrate [Fig. 6(a)–(c)] to determine the ground-state location of a Ga atom to nucleate on the SiC substrate. Each model was fully optimized to acquire their local minimum energy conformations [Fig. 6(a')–(c')]. It is noteworthy that, in such a complex intercalation mechanism, the relative position of defect to Ga and the SiC surface is critical to the Ga nucleation site. Therefore, in the structural-stability calculations in Fig. 6, the defect location on the graphene surface was kept the same, and T1, T4, and H3 sites closest to the defect were identified to reduce the complexity. As illustrated in Fig. 6(a')–(c'), (d), the T4 site was found to be the thermodynamically most favorite nucleation site for Ga at the interface, and the T1 and H3 configurations were relaxed to T4. Additionally, the presence of the defective graphene layer on the top of SiC substantially weakened the Ga-Si bond strength (compare Fig. 4(a) (no graphene) to Fig. 6(d) (with graphene)).

The Ga diffusion from the top of the graphene layer [Fig. 6(e)–(I)] into the SiC/graphene gallery [Fig. 6(e)–(II)] was thermodynamically and kinetically investigated. On the basis of the results, the existence of the SiC substrate underneath graphene breaks mirror symmetry, contrary to the diffusion through free-standing graphene in Fig. 1(d), by generating a lower local minimum than a free-standing graphene layer (referring to the energy difference of 0.9 eV between the configurations I and II as depicted in Fig. 6(e–f). This means that a Ga atom encapsulated at the graphene/SiC interface is thermodynamically more stable than adsorbed on the top of the graphene layer, signifying the necessity of exploiting the SiC substrate during the 2D Ga growth to facilitate the Ga migration into the SiC/graphene interface—this phenomenon is also reported for the Cu, Si, Fe intercalation [26, 38, 53–55]. However, the Ga intercalation through a 5–8–5 vacancy defect into the SiC/graphene interface is kinetically hindered with an energy barrier of 2.1 eV which is the energy required to cleave the reconstructed bond between unpaired C atoms around the defect. As depicted in Fig. 6(f), when Ga atom resides on graphene the bond between undercoordinated C atoms is broken

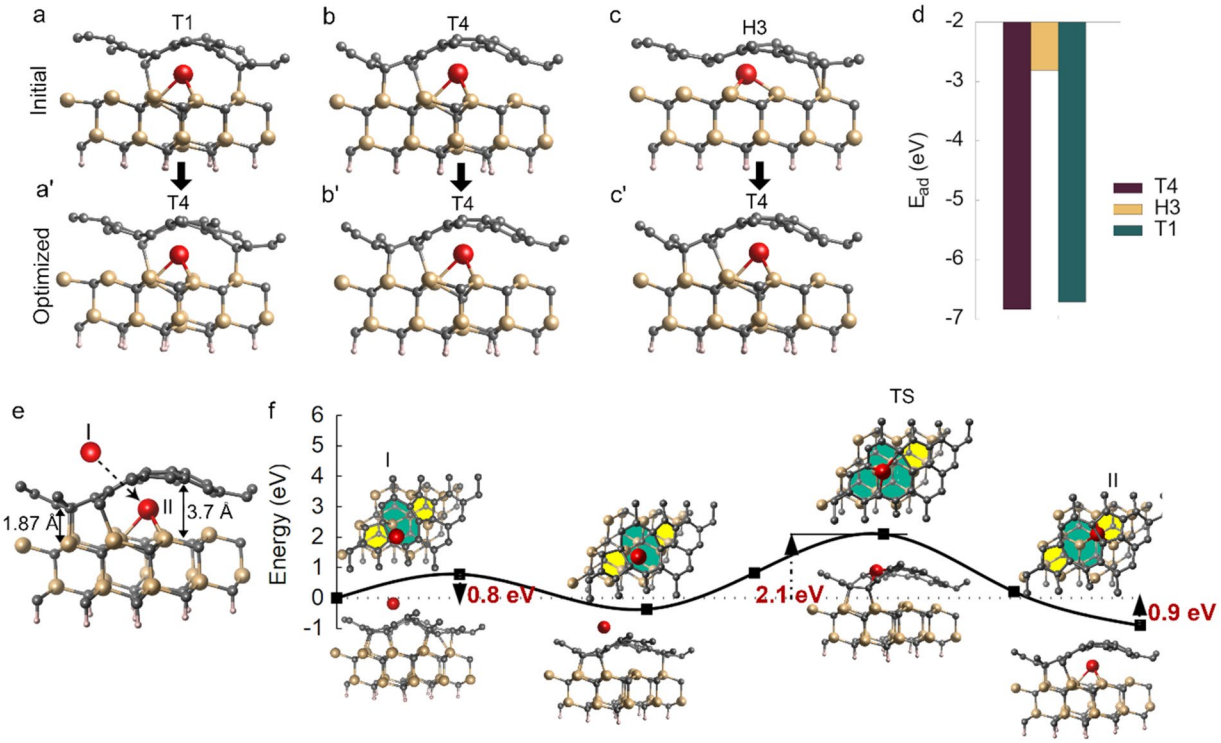

Figure 6: (a), (b), (c) Initial configurations of the Ga-intercalated model where the Ga atom resides on the T4, T1 and H3 sites of the SiC substrate, respectively. (a′, b′, c′) Optimized structures of the models where (b) the T1 and (c) H3 models were relaxed to (b′, c′) the T4 configuration, and (d) the associated the adsorption energies (E_{ad}) of Ga on the SiC surface. (e) The ball-stick representation of the Ga penetration through defective epilayer graphene at the heterointerface of SiC/graphene with the closest and farest interlayer distances of 1.87 and 3.7 Å, respectively, and (f) the associated diffusion pathway. During the intercalation, Ga encounters two kinetic barriers – the first one is 0.8 eV which is required to cleave the reconstructed bond between the graphene sheet and the SiC surface. When Ga resides at the 5–8–5 defect in graphene by breaking one of the reconstructed bonds between unpaired C atoms, it encounters the second barrier of 2.1 eV.

and C-dangling atoms bind to the Ga atom, called a transition state (TS). In case of forcing the Ga atom to penetrate beneath the graphene, the system lowers its energy by reforming the bond between the C-dangling bond where five-membered ring formation occurs and the defect transforms back to 5–8–5, and the Ga atom deposits on the most stable T4 site of the SiC surface. Additionally, similar to the observation in Ref. [26], the Ga intercalation results in the partially Si–C bond cleavage at the interface, then 0.6 Å lifting of the graphene layer—the max interlayer separation between graphene and SiC shown shifts from 3.1 to 3.7 Å [compare Figs. 5(c) and 4(e)]—but there still exist C-Si bonds at the interface [Fig. 6(e)]. In a nutshell, the results on the kinetically hindered Ga intercalation through SV (Fig. 1) and DV [Fig. 6(f) suggest exploiting multivacancy defect (> DV) in graphene to drive the Ga penetration at the interface, in line with the previous studies [11, 24, 25, 28].

Conclusions

Two-dimensional (2D) gallium (Ga) growth from elemental sources has gained increasing attention from the material science community and has been successfully fabricated at the half van der Waals interface of graphene/SiC. However, there is still a lack of theoretical studies on the Ga interaction with graphene and the SiC substrate during the growth. In response to this urgent need, this study provides a detailed theoretical insight into the atomistic mechanism of the Ga intercalation at the graphene/SiC interface through defective graphene and the Ga deposition on the SiC substrate. The first-principles calculations presented here show that single vacancy (SV) and divacancy (DV) strongly draw a Ga atom to the graphene surface. However, Ga encounters a kinetic barrier of 1.02 eV during its penetration through a free-standing graphene layer with an SV defect while DV leads to a nearly "barrierless" diffusion. Additionally, similar to the pristine case, the presence of the reconstructed divacancies (5–8–5 and 555–777) on graphene results in the physisorption of Ga on the surface due to the Jahn teller distortion observed on the graphene models which is an effect stabilizing the graphene sheet by means of the bond reconstruction between C-dangling atoms around the defect. As a next step, a Ga atom was introduced on different symmetry-allowed sites of the SiC surface in the absence of the graphene layer: one-fold coordinated site on the topmost Si atom (T1), four-fold coordinated hcp site above a carbon atom of the first layer

of the SiC substrate (T4), three-fold coordinated fcc site above a carbon atom of the second layer (H3) and bond-centered site and located between two adjacent silicon atoms (BC). A planar bilayer SiC substrate without H-passivation favors the BC site for the Ga adsorption. The T4 site of the SiC substrate (with only its bottom side passivated by H) and the H3 site of the SiC substrate (with both bottom and topsides passivated by H) were found the thermodynamically most stable adsorption sites for Ga. At the final stage, a graphene layer with DV was introduced on the top of the SiC substrate where the Si-dangling bonds on the SiC surface were left unsaturated to allow the graphene sheet to bind to the substrate during the relaxation—thus, mimicking the actual experimental conditions. During the structural relaxation of the graphene/SiC system without Ga, DV undergoes the Jahn Teller distortion and transforms to a 5–8–5 defect. An isolated Ga atom was further introduced on the T1, T4, H3, and BC sites of the SiC substrate, similar to the case without graphene, and the T4 site was determined as the thermodynamically most stable adsorption site. Additionally, the system where a Ga atom occupies the T4 site of the SiC surface at the interface results in lower energy than the system where a Ga atom was introduced above the graphene sheet with a vacancy defect, indicating that a Ga atom encapsulated at the graphene/SiC interface is thermodynamically more stable than adsorbed on the top of the graphene layer. This signifies the necessity of exploiting the SiC substrate during the 2D Ga growth to facilitate the Ga migration into the SiC/graphene interface. However, in the presence of SiC, the Ga intercalation through the 5–8–5 defect encounters the barrier of 2.1 eV because of the C–C bond cleavage of the 5–8–5 ring, followed by the C-Ga bond formation. All these results together indicate that SV and DV defects are kinetically hindered, and Ga metals require larger-sized defects than a divacancy to intercalate at the heterointerface of graphene and SiC.

Materials and methods

Ab-initio calculations were conducted using Quantum Espresso [56, 57] to investigate the coupled effect of graphene defects and the SiC substrate on the Ga intercalation. In these calculations, the electron-ionic core relation was represented using a Projected Augmented Potential [58, 59], and exchange–correlation interactions were treated using the parametrization of the Perdew-Burke-Ernzerhof [60, 61]. A $5\times5\times1$ k-point mesh within Gamma centered Monkhorst–Pack scheme was applied to Brillouin Zone integration with a kinetic energy cut-off of 40 Ry and a density cutoff of 400 Ry. The Marzari–Vanderbilt cold smearing scheme was utilized with a broadening of 0.01 Ry. In the geometry optimizations, the system was allowed to relax fully using a Broyden–Fletcher–Goldfarb–Shanno algorithm along with the total energy threshold of 0.0001 Ry and the force threshold of 0.001 Ry/Å. Periodic boundary conditions were applied along the three directions of the space. A vacuum layer of 20 Å was inserted in the direction of normal to the graphene sheets to minimize the spurious interactions by the periodic repetitions. For the SiC/graphene model where graphene is rotated by 0° with respect to the SiC substrate as shown in Fig. 6(c), the graphene cap layer with the dimensions of 9.85×9.85 Å^2 is compressed by about 6% to match the lateral size of the Si-terminated SiC (0001) substrate with the dimensions of 9.23×9.23 Å^2. To reduce the computational cost, in the calculations a two-layer thick SiC was adopted and the bottom layer of the SiC/graphene model was hydrogenated. Note that the size of the numerical uncertainties can depend on the model size, the number of SiC layers, DFT parameters, etc.—therefore, the calculation methodology and the accuracy level of pseudopotentials are critical to obtaining accurate models. The models in the figures were visualized using VESTA [62] software. Energy barriers were calculated by the climbing image nudged elastic band (CI-NEB) method [63]. A force-based optimizer of Quick-min was used to relax the trajectory through CI-NEB sampling until the net force acting on each image reached 0.01 eV/Å. The NEB calculations were realized in two stages: (i) No-climbing image: an approximate pathway including seven replicas between the optimized reactant and product was first mapped out before starting the search for the transition state. At this stage, the Broyden algorithm was utilized in order to avoid oscillations in the calculated atomic energies. (ii) Climbing image: Following the convergence of the first stage with a no-climbing image, the climbing image option was turned on to accurately locate the transition state with accurate potential energy by eliminating the effect of spring forces and allowing replicas to climb freely to the local maximum energy state, in other words, the transition state.

Acknowledgments

The author thanks to Prof. Adri van Duin for the fruitful discussions.

Funding

This work was financially supported by the National Science Foundation (NSF) through the Pennsylvania State University 2D Crystal Consortium—Materials Innovation Platform (2DCC-MIP) under the NSF cooperative agreement DMR-1808900.

Data availability

The data are available upon reasonable request from the corresponding author (N.N.).

Declarations

Conflict of interest The author declares no conflict of interests.

References

1. S. Chabi, K. Kadel, Two-dimensional silicon carbide: emerging direct band gap semiconductor. Nanomaterials (2020). https://doi.org/10.3390/nano10112226
2. A. Zavabeti, A. Jannat, L. Zhong, A.A. Haidry, Z. Yao, J.Z. Ou, Two-dimensional materials in large-areas: synthesis, properties and applications. Nano-Micro Lett. **12**(1), 66 (2020). https://doi.org/10.1007/s40820-020-0402-x
3. Z.Y. Al Balushi et al., Two-dimensional gallium nitride realized via graphene encapsulation. Nat. Mater. **15**(11), 1166–1171 (2016). https://doi.org/10.1038/nmat4742
4. Y.G. Cao, M.H. Xie, Y. Liu, Y.F. Ng, H.S. Wu, S.Y. Tong, InN island shape and its dependence on growth condition of molecular-beam epitaxy. Appl. Phys. Lett. **83**(25), 5157–5159 (2003). https://doi.org/10.1063/1.1635077
5. V. Narayanan, K. Lorenz, W. Kim, S. Mahajan, Gallium nitride epitaxy on (0001) sapphire. Philos. Mag. A **82**(5), 885–912 (2002). https://doi.org/10.1080/01418610208240008
6. N. Itagaki et al., Growth of single crystalline films on lattice-mismatched substrates through 3D to 2D mode transition. Sci. Rep. **10**(1), 4669 (2020). https://doi.org/10.1038/s41598-020-61596-w
7. C. Adelmann, B. Daudin, R.A. Oliver, G.A.D. Briggs, R.E. Rudd, Nucleation and growth of $\mathrm{GaN}/\mathrm{AlN}$ quantum dots. Phys. Rev. B **70**(12), 125427 (2004). https://doi.org/10.1103/PhysRevB.70.125427
8. L.W. Liu et al., Growth and structural properties of Pb Islands on epitaxial graphene on Ru(0001). J. Phys. Chem. C **117**(44), 22652–22655 (2013). https://doi.org/10.1021/jp404190c
9. A.C. Levi, M. Kotrla, Theory and simulation of crystal growth. J. Phys. Condens. Matter **9**(2), 299–344 (1997). https://doi.org/10.1088/0953-8984/9/2/001
10. A. Braun, M. Diale, J.B. Malherbe, M. Braun, Introduction. J. Mater. Res. **32**(21), 3921–3923 (2017). https://doi.org/10.1557/jmr.2017.426
11. N. Briggs et al., Atomically thin half-van der Waals metals enabled by confinement heteroepitaxy. Nat. Mater. (2020). https://doi.org/10.1038/s41563-020-0631-x
12. M. Rajapakse et al., Intercalation as a versatile tool for fabrication, property tuning, and phase transitions in 2D materials. Npj 2D Mater Appl. **5**(1), 1–21 (2021). https://doi.org/10.1038/s41699-021-00211-6
13. M.S. Stark, K.L. Kuntz, S.J. Martens, S.C. Warren, Intercalation of layered materials from bulk to 2D. Adv. Mater. **31**(27), 1808213 (2019). https://doi.org/10.1002/adma.201808213
14. B. Pécz, G. Nicotra, F. Giannazzo, R. Yakimova, A. Koos, A. Kakanakova-Georgieva, Indium nitride at the 2D Limit. Adv. Mater. **33**(1), 2006660 (2021). https://doi.org/10.1002/adma.202006660
15. A. Kakanakova-Georgieva et al., Nanoscale phenomena ruling deposition and intercalation of AlN at the graphene/SiC interface. Nanoscale **12**(37), 19470–19476 (2020). https://doi.org/10.1039/D0NR04464D
16. S. Rajabpour et al., Tunable 2D group-III metal alloys. Adv. Mater. (2021). https://doi.org/10.1002/adma.202104265
17. F. Bisti et al., Electronic and geometric structure of graphene/SiC(0001) decoupled by lithium intercalation. Phys. Rev. B **91**(24), 245411 (2015). https://doi.org/10.1103/PhysRevB.91.245411
18. Y.-P. Lin, Y. Ksari, J.-M. Themlin, Hydrogenation of the buffer-layer graphene on 6H-SiC (0001): a possible route for the engineering of graphene-based devices. Nano Res. **8**(3), 839–850 (2015). https://doi.org/10.1007/s12274-014-0566-0
19. C. Riedl, C. Coletti, T. Iwasaki, A.A. Zakharov, U. Starke, Quasi-free-standing epitaxial graphene on SiC obtained by hydrogen intercalation. Phys. Rev. Lett. **103**(24), 246804 (2009). https://doi.org/10.1103/PhysRevLett.103.246804
20. W. Tian, W. Li, W. Yu, X. Liu, A review on lattice defects in graphene: types, generation, effects and regulation. Micromachines (2017). https://doi.org/10.3390/mi8050163
21. F. Banhart, J. Kotakoski, A.V. Krasheninnikov, Structural defects in graphene. ACS Nano **5**(1), 26–41 (2011). https://doi.org/10.1021/nn102598m
22. J.C. Meyer, C. Kisielowski, R. Erni, M.D. Rossell, M.F. Crommie, A. Zettl, Direct imaging of lattice atoms and topological defects in graphene membranes. Nano Lett. **8**(11), 3582–3586 (2008). https://doi.org/10.1021/nl801386m
23. J. Ma, D. Alfè, A. Michaelides, E. Wang, Stone-Wales defects in graphene and other planar $s{p}^{2}$-bonded materials. Phys. Rev. B **80**(3), 033407 (2009). https://doi.org/10.1103/PhysRevB.80.033407
24. N. Nayir et al., Atomic-scale probing of defect-assisted Ga intercalation through graphene using ReaxFF molecular dynamics simulations. Carbon **190**, 276–290 (2022). https://doi.org/10.1016/j.carbon.2022.01.005
25. Y. Han, J.W. Evans, M.C. Tringides, Dy adsorption on and intercalation under graphene on 6H-SiC(0001) surface from first-principles calculations. Phys. Rev. Mater. **5**(7), 074004 (2021). https://doi.org/10.1103/PhysRevMaterials.5.074004
26. Y. Orimoto, K. Otsuka, K. Yagyu, H. Tochihara, T. Suzuki, Y. Aoki, Theoretical study of Cu intercalation through a defect in zero-layer graphene on SiC surface. J. Phys. Chem. C **121**(13), 7294–7302 (2017). https://doi.org/10.1021/acs.jpcc.7b00314
27. F. Yao et al., Diffusion mechanism of lithium ion through basal plane of layered graphene. J. Am. Chem. Soc. **134**(20), 8646–8654 (2012). https://doi.org/10.1021/ja301586m

28. Y. Han, A. Lii-Rosales, M.C. Tringides, J.W. Evans, P.A. Thiel, Energetics of Cu adsorption and intercalation at graphite step edges. Phys. Rev. B **99**(11), 115415 (2019). https://doi.org/10.1103/PhysRevB.99.115415
29. Y. Liu et al., Mechanism of metal intercalation under graphene through small vacancy defects. J. Phys. Chem. C **125**(12), 6954–6962 (2021). https://doi.org/10.1021/acs.jpcc.1c00814
30. A. Lii-Rosales et al., Encapsulation of metal nanoparticles at the surface of a prototypical layered material. Nanoscale **13**(3), 1485–1506 (2021). https://doi.org/10.1039/D0NR07024F
31. M. Büttner, P. Choudhury, J. Karl Johnson, J.T. Yates, Vacancy clusters as entry ports for cesium intercalation in graphite. Carbon **49**(12), 3937–3952 (2011). https://doi.org/10.1016/j.carbon.2011.05.032
32. Y. Han, J.W. Evans, M.C. Tringides, Thermodynamics and kinetics of H adsorption and intercalation for graphene on 6H-SiC(0001) from first-principles calculations. J. Vac. Sci. Technol. A **40**(1), 012202 (2022). https://doi.org/10.1116/6.0001343
33. W. Zhang, A.C.T. van Duin, Atomistic-scale simulations of the graphene growth on a silicon carbide substrate using thermal decomposition and chemical vapor deposition. Chem. Mater. **32**(19), 8306–8317 (2020). https://doi.org/10.1021/acs.chemmater.0c02121
34. E. Voloshina, K. Rosciszewski, B. Paulus, First-principles study of the connection between structure and electronic properties of gallium. Phys. Rev. B **79**(4), 045113 (2009). https://doi.org/10.1103/PhysRevB.79.045113
35. B.Q. Song, L.D. Pan, Penetration of the first-two-row elements through mono-layer graphene. Carbon **109**, 117–123 (2016). https://doi.org/10.1016/j.carbon.2016.07.065
36. J. Emsley, *The elements*, 3rd edn. (Clarendon Press, Oxford, 1998)
37. W. Li, L. Huang, M.C. Tringides, J.W. Evans, Y. Han, Thermodynamic preference for atom adsorption on versus intercalation into multilayer graphene. J. Phys. Chem. Lett. **11**(22), 9725–9730 (2020). https://doi.org/10.1021/acs.jpclett.0c02887
38. G. Li et al., Role of cooperative interactions in the intercalation of heteroatoms between graphene and a metal substrate. J. Am. Chem. Soc. **137**(22), 7099–7103 (2015). https://doi.org/10.1021/ja5113657
39. J. Rohrer, E. Ziambaras, P. Hyldgaard, Relative stability of $6H$-SiC$\{0001\}$ surface terminations and formation of graphene overlayers by Si evaporation. *ArXiv11022111 Cond-Mat*. (2011.) http://arxiv.org/abs/1102.2111. Accessed 29 Nov 2021.
40. R. Gutzler, J.C. Schön, Two-dimensional silicon-carbon compounds: structure prediction and band structures. Z. Für Anorg. Allg. Chem. **643**(21), 1368–1373 (2017). https://doi.org/10.1002/zaac.201700258
41. Y. Miyamoto, B.D. Yu, Computational designing of graphitic silicon carbide and its tubular forms. Appl. Phys. Lett. **80**(4), 586–588 (2002). https://doi.org/10.1063/1.1445474
42. M. Yu, C.S. Jayanthi, S.Y. Wu, bonding nature, structural optimization, and energetics studies of SiC graphitic-like layer structures and single/double walled nanotubes. Phys. Rev. B **82**(7), 075407 (2010). https://doi.org/10.1103/PhysRevB.82.075407
43. C.L. Freeman, F. Claeyssens, N.L. Allan, J.H. Harding, Graphitic nanofilms as precursors to wurtzite films: theory. Phys. Rev. Lett. **96**(6), 066102 (2006). https://doi.org/10.1103/PhysRevLett.96.066102
44. T. Susi et al., Computational insights and the observation of SiC nanograin assembly: towards 2D silicon carbide. Sci. Rep. **7**(1), 4399 (2017). https://doi.org/10.1038/s41598-017-04683-9
45. Z. Zhao, Y. Yong, Q. Zhou, Y. Kuang, X. Li, Gas-sensing properties of the SiC monolayer and bilayer: a density functional theory study. ACS Omega **5**(21), 12364–12373 (2020). https://doi.org/10.1021/acsomega.0c01084
46. L. Pan et al., First-principles study of monolayer and bilayer honeycomb structures of group-IV elements and their binary compounds. Phys. Lett. A **375**(3), 614–619 (2011). https://doi.org/10.1016/j.physleta.2010.11.062
47. L. Yuan, Z. Li, J. Yang, Hydrogenated bilayer wurtzite SiC nanofilms: a two-dimensional bipolar magnetic semiconductor material. Phys. Chem. Chem. Phys. **15**(2), 497–503 (2012). https://doi.org/10.1039/C2CP43129G
48. G. Lee, J. Kim, K. Kim, J.W. Han, Precise control of defects in graphene using oxygen plasma. J. Vac. Sci. Technol. A **33**(6), 060602 (2015). https://doi.org/10.1116/1.4926378
49. N. Ferralis, R. Maboudian, C. Carraro, Evidence of structural strain in epitaxial graphene layers on 6H-SiC(0001). Phys. Rev. Lett. **101**(15), 156801 (2008). https://doi.org/10.1103/PhysRevLett.101.156801
50. Z.H. Ni et al., Raman spectroscopy of epitaxial graphene on a SiC substrate. Phys. Rev. B **77**(11), 115416 (2008). https://doi.org/10.1103/PhysRevB.77.115416
51. I. Shtepliuk, R. Yakimova, Interaction of H and Li with epitaxial graphene on SiC: a comparative analysis by first principles study. Appl. Surf. Sci. **568**, 150988 (2021). https://doi.org/10.1016/j.apsusc.2021.150988
52. T. Cavallucci, V. Tozzini, Intrinsic structural and electronic properties of the buffer layer on silicon carbide unraveled by density functional theory. Sci Rep (2018). https://doi.org/10.1038/s41598-018-31490-7
53. Y. Cui et al., An exchange intercalation mechanism for the formation of a two-dimensional Si structure underneath graphene. Nano Res. **5**(5), 352–360 (2012). https://doi.org/10.1007/s12274-012-0215-4
54. A. Lii-Rosales et al., Formation of multilayer cu islands embedded beneath the surface of graphite: characterization and fundamental insights. J. Phys. Chem. C **122**(8), 4454–4469 (2018). https://doi.org/10.1021/acs.jpcc.7b12533

55. A. Lii-Rosales et al., Fabricating Fe nanocrystals via encapsulation at the graphite surface. J. Vac. Sci. Technol. A **37**(6), 061403 (2019). https://doi.org/10.1116/1.5124927
56. P. Giannozzi et al., QUANTUM ESPRESSO: a modular and open-source software project for quantum simulations of materials. J. Phys. Condens. Matter **21**(39), 395502 (2009). https://doi.org/10.1088/0953-8984/21/39/395502
57. P. Giannozzi et al., Advanced capabilities for materials modelling with Quantum ESPRESSO. J. Phys. Condens. Matter **29**(46), 465901 (2017). https://doi.org/10.1088/1361-648X/aa8f79
58. G. Kresse, D. Joubert, From ultrasoft pseudopotentials to the projector augmented-wave method. Phys. Rev. B **59**(3), 1758–1775 (1999). https://doi.org/10.1103/PhysRevB.59.1758
59. P.E. Blöchl, Projector augmented-wave method. Phys. Rev. B **50**(24), 17953–17979 (1994). https://doi.org/10.1103/PhysRevB.50.17953
60. J.P. Perdew, K. Burke, M. Ernzerhof, Generalized gradient approximation made simple. Phys. Rev. Lett. **77**(18), 3865–3868 (1996). https://doi.org/10.1103/PhysRevLett.77.3865
61. J.P. Perdew, K. Burke, M. Ernzerhof, Generalized gradient approximation made simple [Phys. Rev. Lett. 77, 3865 (1996)]. Phys. Rev. Lett. **78**(7), 1396–1396 (1997). https://doi.org/10.1103/PhysRevLett.78.1396
62. K. Momma, F. Izumi, VESTA 3 for three-dimensional visualization of crystal, volumetric and morphology data. J. Appl. Crystallogr. **44**(6), 1272–1276 (2011). https://doi.org/10.1107/S0021889811038970
63. G. Henkelman, B.P. Uberuaga, H. Jónsson, A climbing image nudged elastic band method for finding saddle points and minimum energy paths. J. Chem. Phys. **113**(22), 9901–9904 (2000). https://doi.org/10.1063/1.1329672